THE JOURNAL OF BIOLOGICAL CHEMISTRY VOL. 288, NO. 51, pp. 36215–36225, December 20, 2013

The Structural Basis for Endotoxin-induced Allosteric Regulation of the Toll-like Receptor 4 (TLR4) Innate Immune Receptor*

Received for publication, July 16, 2013, and in revised form, October 30, 2013 Published, JBC Papers in Press, October 30, 2013, DOI 10.1074/jbc.M113.501957

Teresa Paramo[‡], Thomas J. Piggot[§1], Clare E. Bryant[¶2], and Peter J. Bond[‡3]

From the [‡]Unilever Centre for Molecular Science Informatics, Department of Chemistry, University of Cambridge, Lensfield Road, Cambridge CB2 1EW, United Kingdom, the [§]School of Chemistry, University of Southampton, Highfield, Southampton SO17 1BJ, United Kingdom, and the [¶]Department of Veterinary Medicine, University of Cambridge, Madingley Road, Cambridge CB3 0ES, United Kingdom

Background: Toll-like receptor 4 (TLR4) in complex with MD-2 stimulates innate immunological pathways in response to bacterial lipopolysaccharide (LPS).
Results: Molecular simulations reveal the mechanism of TLR4 complex signaling in response to agonists or antagonists.
Conclusion: Conserved clamshell motions in MD-2 allosterically signal ligand-bound state via the conserved phenylalanine 126 residue to TLR4.
Significance: The structural basis for molecular switching during endotoxin-induced TLR4 activation is revealed in atomic detail.

As part of the innate immune system, Toll-like receptor 4 (TLR4) recognizes bacterial cell surface lipopolysaccharide (LPS) by forming a complex with a lipid-binding co-receptor, MD-2. In the presence of agonist, TLR4·MD-2 dimerizes to form an active receptor complex, leading to initiation of intracellular inflammatory signals. TLR4 is of great biomedical interest, but its pharmacological manipulation is complicated because even subtle variations in the structure of LPS can profoundly impact the resultant immunological response. Here, we use atomically detailed molecular simulations to gain insights into the nature of the molecular signaling mechanism. We first demonstrate that MD-2 is extraordinarily flexible. The "clamshell-like" motions of its β-cup fold enable it to sensitively match the volume of its hydrophobic cavity to the size and shape of the bound lipid moiety. We show that MD-2 allosterically transmits this conformational plasticity, in a ligand-dependent manner, to a phenylalanine residue (Phe-126) at the cavity mouth previously implicated in TLR4 activation. Remarkably, within the receptor complex, we observe spontaneous transitions between active and inactive signaling states of Phe-126, and we confirm that Phe-126 is indeed the "molecular switch" in endotoxic signaling.

The innate immune system represents the initial gateway to almost all mammalian inflammatory responses against invading microbes. Members of the transmembrane Toll-like receptor (TLR)[4] family are specialized for recognizing pathogen-associated molecular patterns with diverse structural and physiochemical properties, ranging from microbial cell wall components to nucleic acids (1). A key pathogen-associated molecular pattern is lipopolysaccharide (LPS) from the outer membranes of Gram-negative bacteria. LPS is a powerful activator of the innate immune response, and in sepsis overstimulation can lead to endotoxicity and death (2). LPS recognition is carried out by TLR4 in concert with a series of accessory proteins that amplify the response (3). LPS-binding protein and CD14 help to transfer LPS from bacterial membranes or aggregates in serum to myeloid differentiation factor 2 (MD-2) (4). Unlike the rest of the TLR family, TLR4 does not recognize ligand in isolation, but when bound to MD-2. Upon formation of an active receptor complex at the cell surface, it is presumed that conformational changes lead to transmission of an activating signal to the intracellular Toll-interleukin 1 receptor domains, resulting in recruitment of adaptor proteins, and subsequent MAL-MyD88 and TRAM-TRIF-dependent inflammatory responses (3, 5).

LPS is a glycolipid, composed of an oligosaccharide core and a highly variable O antigen polysaccharide component, along with a hydrophobic lipid A segment containing multiple lipid acyl tails and a phosphorylated glucosamine disaccharide headgroup (6). The lipid A core of LPS is responsible for much of its bioactivity. The structure and composition of lipid A vary among bacterial species, and even subtle variations can profoundly impact the stimulatory activity of TLR4. For example, whereas the highly agonistic *Escherichia coli* lipid A (LPA) is hexaacylated, its biosynthetic intermediate lipid IVa (LPIVa) is tetraacylated and acts as an agonist in mice and horses (7) but as an antagonist in humans (8). The tetraacylated synthetic compound eritoran (Erit) appears to be a strong antagonist in all species (9, 10). Monophosphoryl lipid A (MPLA) resembles

* This work was supported by Unilever (to P. J. B. and T. P.).
[1] Present address: Detection Department, Defence Science and Technology Laboratory, Porton Down, Salisbury, Wiltshire SP4 0JQ, United Kingdom.
[2] Biotechnology and Biological Sciences Research Council (BBSRC) Research Development Fellow.
[3] To whom correspondence should be sent: Bioinformatics Institute (A*STAR), 30 Biopolis St, 07-01 Matrix, Singapore 138671. Tel.: 65-6478-8378; E-mail: peterjb@bii.a-star.edu.sg.
[4] The abbreviations used are: TLR, Toll-like receptor; BSA, buried surface area; Erit, eritoran; iMD-2, isolated MD-2; iTLR4, isolated TLR4; LPA, lipid A; LPIVa, lipid IVa; LRR, leucine-rich repeat; MD-2, myeloid differentiation factor 2; MD-2c, closed MD-2; MD-2o, open MD-2; MPLA, monophosphoryl lipid A; Myr, myristate; PDB, Protein Data Bank; r.m.s.d., root mean square deviation.

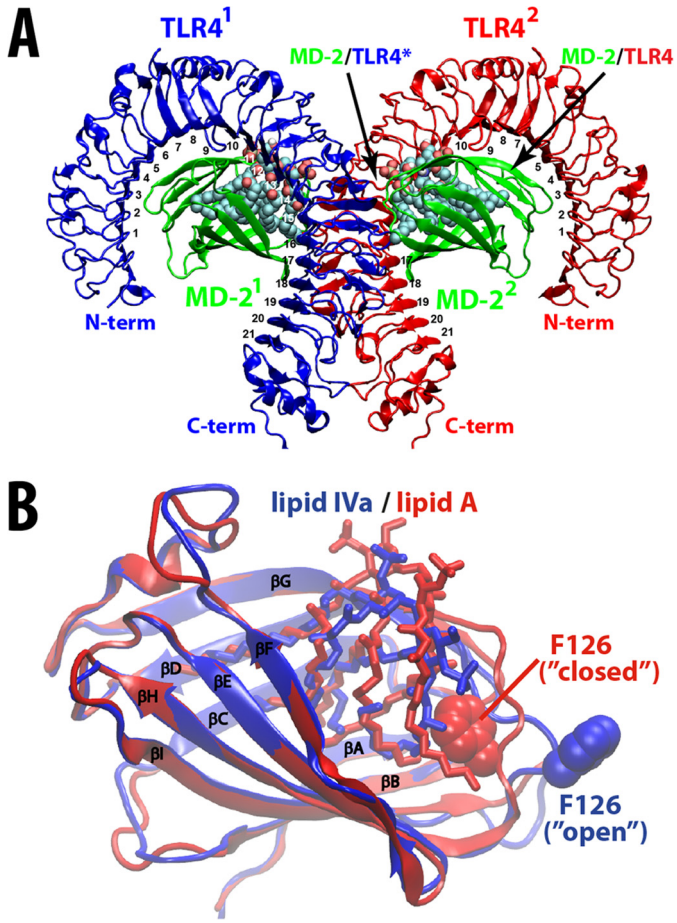

FIGURE 1. **TLR4 and MD-2 structures.** *A*, active LPA-bound $[TLR4{\cdot}MD\text{-}2]_2$ heterotetrameric complex (13), with protein shown in *schematic* format. Each TLR4 (*red*/*blue*) and MD-2 (*green*) chain is labeled, and bound *LPA* is shown in *spacefill* format (*CPK colors*). Key heterodimeric interfaces, TLR4 termini, and LRRs are *highlighted*. *B*, overlay of the closed conformation of MD-2 (MD-2c) bound to LPA (13) shown in *red*, and the open conformation of MD-2 (MD-2o) bound to LPIVa (14) shown in *blue*. Protein is shown in *schematic* format, with ligand (*wireframe*) and Phe-126 (*spacefill*) *highlighted*.

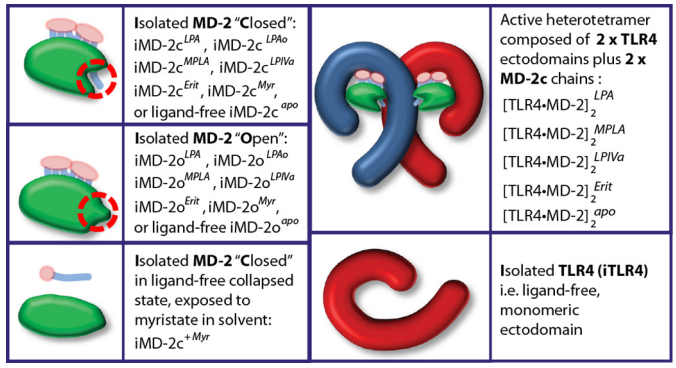

FIGURE 2. **Overview of each simulation system and corresponding naming convention, with domains represented *schematically* and *colored* as in Fig. 1.** In isolated MD-2, the state of the gating loop containing Phe-126 is highlighted with a *red dashed circle*.

LPA but has a singly phosphorylated headgroup; it acts as a partial agonist by activating the TRIF pathway without stimulating the MyD88 response (11).

A variety of recent biochemical and crystallographic data have provided insight into the molecular mechanisms of LPS recognition and signaling by TLR4. Like all TLRs, TLR4 has a curved, solenoidal ectodomain containing multiple leucine-rich repeat (LRR) domains (12, 13). MD-2 has been shown to form a TLR4·MD-2 heterodimer by binding to the amino-terminal and central LRRs of TLR4, at the "primary interface" (12). Moreover, LPS-bound MD-2 facilitates formation of the active receptor complex (13), consisting of a "dimer of dimers," *i.e.* $[TLR4{\cdot}MD\text{-}2]_2$, stabilized by new interactions between MD-2/LPS and the carboxyl-terminal LRRs on the opposing TLR4 chain (referred to here as TLR4*), at the "secondary interface" (Fig. 1*A*).

Several crystal structures have confirmed that MD-2 adopts a nine-stranded immunoglobulin-like β-cup fold (with successive β-strands referred to as βA, βB, βC, etc.), composed of two curved β-sheets that house a deep hydrophobic pocket, specialized for binding the acyl tails of a range of lipid moieties (12–14). A variety of evidence suggests that one part of MD-2 plays a particularly important role in activation of TLR4, namely, the flexible βG-βH loop connecting strands βG and βH, which contains a key phenylalanine residue, Phe-126, located near the cavity mouth (Fig. 1*B*). An F126A mutant does not prevent ligand binding, but impairs formation of the active receptor complex and hence endotoxin-dependent signaling (15). Comparison of available structural data reveals that the βG-βH loop is conformationally dynamic, adopting an "open conformation" in the presence of nonactivating ligands, with Phe-126 oriented outside of the binding pocket, exposed to solvent (12, 14), and an alternative "closed conformation" in the presence of LPS, with Phe-126 pointing into the cavity, facilitating interaction with an exposed lipid tail (Fig. 1*B*) that may stabilize contacts between TLR4* and MD-2 in the $[TLR4{\cdot}MD\text{-}2]_2$ complex (13). NMR analysis combined with metabolic labeling of a hexaacylated agonist recently provided support for the idea that Phe-126 acts as a "hydrophobic switch" (16). In both MD-2 and its F126A mutant, a single fatty acyl chain was shown to be more susceptible to paramagnetic attenuation, independent of TLR4 association, whereas the local environment of bound lipid tails was altered in the F126A mutant compared with wild type, suggesting that Phe-126 may be important in promoting formation of the active $[TLR4{\cdot}MD\text{-}2]_2$ complex (16).

Despite the evident progress in characterizing TLR4 activation, there still remain outstanding questions. In particular, we lack information at atomic resolution about the nature of the agonist-bound MD-2 state prior to complex formation with TLR4, or conversely, an antagonist-bound receptor complex intermediate, both of which would help to clarify the nature of the "switch" in TLR4 molecular signaling. To gain further insights into the molecular signaling process, we now report an atomically detailed molecular simulation study of isolated MD-2 (iMD-2), as well as the entire active $[TLR4{\cdot}MD\text{-}2]_2$ receptor complex, comprising almost half a million atoms (Fig. 2). The results obtained from this substantial computational effort, which constitutes ~3 μs of simulation time (Fig. 2), allow us to formulate detailed mechanistic hypotheses for the process of TLR4 (de)activation in the context of available experimental data.

By first considering solvated human iMD-2 in the presence of a range of ligands (Fig. 3*A* and see Table 1), including agonistic

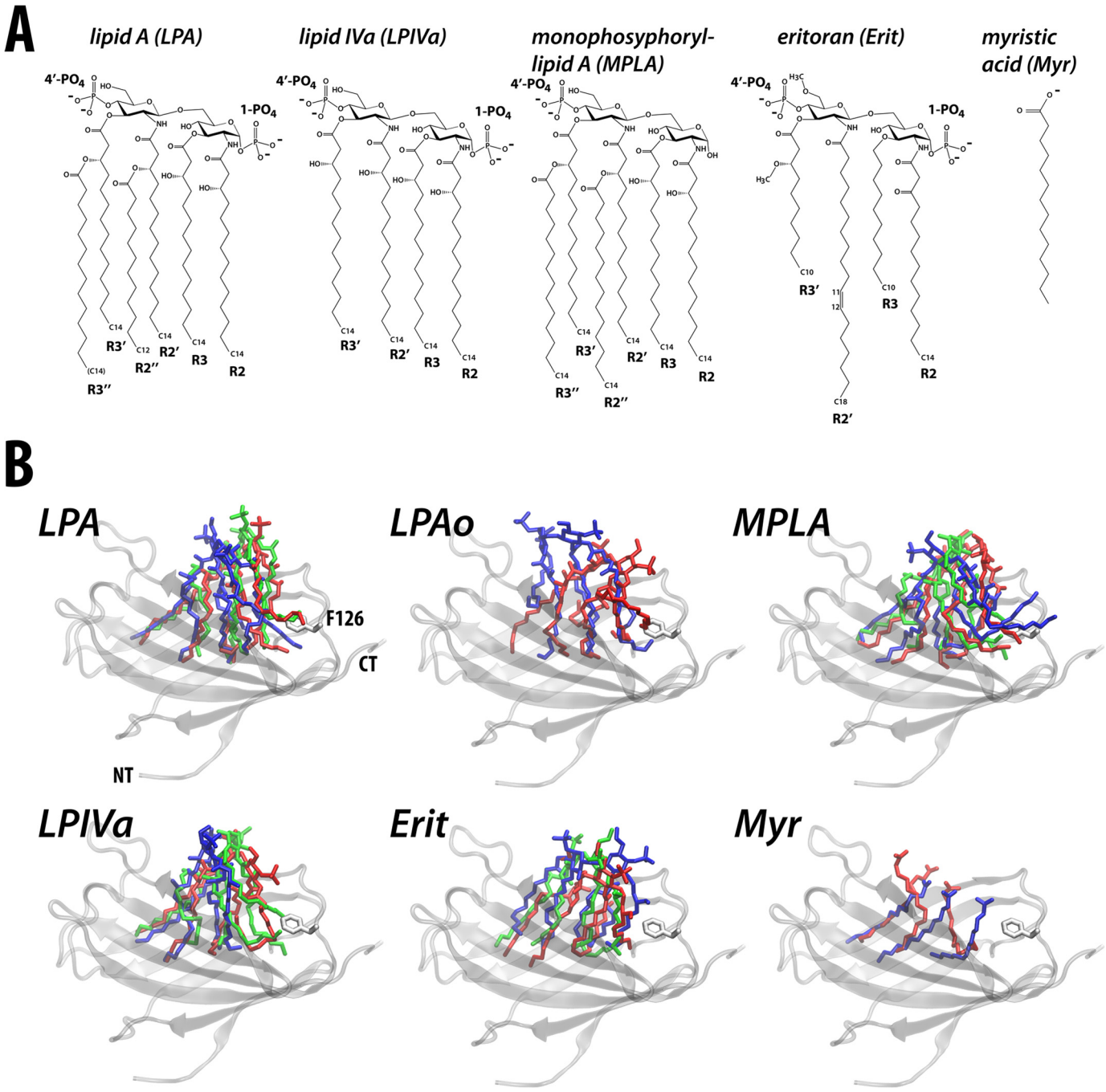

FIGURE 3. **MD-2 ligand binding.** *A*, chemical structures of ligands employed in this study. *B*, MD-2c structure (*transparent schematic* format) with bound ligand shown in *wireframe* format. For each system, the initial location of bound ligand (*red*) is shown, with the final conformation in iMD-2 (*blue*) and $[TLR4{\cdot}MD\text{-}2]_2$ (*green*) simulations overlaid. The initial conformation of Phe-126 is shown in *gray wireframe* format, and for the LPA-bound system, Phe-126 and amino (*NT*) and carboxyl (*CT*) termini are labeled.

LPA, partial agonist MPLA, antagonists LPIVa and Erit, and the inactive ligand myristate (Myr), we verify that lipid tail exposure precedes TLR4 association and is not exclusive to the agonist-bound state (16). Furthermore, we provide support for the notion that Phe-126 acts as a hydrophobic switch (16) within the βG-βH "gating loop." We show that in both the closed (iMD-2c) and open (iMD-2o) gating loop states, the iMD-2 cavity is extraordinarily malleable, and can undergo "clamshell-like" motions, reversibly adjusting its volume to sensitively match the size and shape of the bound lipid moiety. Strikingly, MD-2 appears to be capable of transmitting the mechanical energy associated with cavity collapse and expansion to the gating loop, allosterically modulating its conformational state and determining potential ligand interactions with Phe-126. Furthermore, the apparent conformational plasticity of MD-2 is shown to be pertinent in the context of the complete $[TLR4{\cdot}MD\text{-}2]_2$ heterotetramer. We directly observe spontaneous switching from the active to inactive signaling state in the absence of agonist (or to an intermediate state in the presence of partial agonist), coupled to destabilization of the receptor

complex. In other words, a glimpse is provided of the Phe-126 molecular switch in action.

COMPUTATIONAL PROCEDURES

Simulation Details—All simulations were performed using GROMACS 4.5 (17). For most systems, the CHARMM22/CMAP all-atom force field (18, 19) was used to represent the protein, with the explicit solvent TIP3P water model. New lipid parameters were based on previously parameterized CHARMM phospholipid and sugar molecules from the CHARMM27 force field. Optimization of these parameters involved testing their performance in reproducing structural and dynamic properties from previous experimental and simulation studies (20) within lipid bilayers, a description of which will be provided in a separate paper. Additional simulations were carried out using other force fields, including AMBER99SB-ILDN (21) with the TIP3P water model, OPLS-AA/L (22) with the TIP4P water model, and GROMOS53A6 (23) with the SPC water model.

All simulations were performed in the NpT ensemble, at a temperature of 298 K and pressure of 1 atm. Temperature and pressure were controlled using the velocity-rescale thermostat (24) and the Parrinello-Rahman barostat using isotropic coupling (25, 26), respectively. Equations of motion were integrated using the leapfrog method with a 2-fs time step, and the LINCS algorithm was used to constrain bond lengths (27). Nonbonded pairlists were generated every 10 steps using a distance cutoff of 1.4 nm. A cutoff of 1.2 nm was used for Lennard-Jones (excluding scaled 1–4) interactions, which were smoothly switched off between 1 and 1.2 nm. Electrostatic interactions were computed using the Particle-Mesh-Ewald algorithm (28) with a real-space cutoff of 1.2 nm.

Simulation analysis was performed using GROMACS and VMD (29). Characterization of the time-dependent shape of the MD-2 binding cavity was performed using in-house code using a voxel size of 0.14 nm (details of the algorithm are to be published separately). Unless otherwise stated, averages ± S.D. were calculated over the last 20 ns of each trajectory.

Simulation Setup—A periodic, truncated octahedral box was used for all systems, with a minimum of 1.5 nm between protein/lipid atoms and the box edges. A heuristic distance-based approach was used to check likely charge states of ionizable residues; as a result, these were all assigned their default ionization states, assuming neutral pH conditions. Each system was solvated via superposition of a preequilibrated box of water molecules. Sodium and chloride ions were added to neutralize any net charge in the system, with a total concentration of ~0.1 M used to mimic physiological salt conditions. Before and after solvation, energy minimization was performed using the steepest descent algorithm to relax any undesirable steric clashes among protein, lipid, and solvent. Subsequently, a solvent equilibration phase was carried out, during which the positions of protein and lipid heavy atoms were gradually released from their initial configuration over 1.5 ns of simulation. Finally, production simulations were run for at least 100 ns.

Starting Structures—The initial human iMD-2c, isolated human TLR4 (iTLR4), and human $[TLR4{\cdot}MD\text{-}2]_2$ systems were obtained from the crystal structure of the active receptor complex bound to *E. coli* LPS (13) (PDB ID code 3FXI). The human iMD-2o systems were based on the structure of MD-2 bound to lipid IVa (14) (PDB ID code 2E59). The iMD-2, iTLR4, and $[TLR4{\cdot}MD\text{-}2]_2$ systems were placed in an octahedral unit cell of dimension ~8 nm (containing ~10,000 waters), 13 nm (~50,000 waters), or ~17 nm (~100,000 waters), respectively.

Ligand-bound conformations were generated on the basis of available crystal structures for LPA (PDB ID code 3FXI) (13), LPIVa (14) (PDB ID code 2E59), Erit (12) (PDB ID code 2Z65), and Myr (14) (PDB ID code 2E56), using pair-wise STAMP structural alignment (30) of MD-2 conformations where appropriate. Systems containing MPLA or LPA in the orientation opposite to that in the 3FXI crystal structure, were built with PyMOL using the available LPS-bound state as a template. Apo state systems were set up by removal of ligand from the open and closed MD-2 crystal structures. Apo simulations were carried out three times to ensure reproducibility; similar results were obtained for all trajectories, so only one is presented in detail. In one of the collapsed, closed apo simulations, the final snapshot was extracted, and six myristate molecules were placed above the mouth of the cavity, prior to further simulation.

RESULTS

Protrusion of a Single Lipid Tail Is Insufficient for Signaling to TLR4—NMR-based relaxation enhancement was recently used to demonstrate the increased solvent accessibility of the mouth-proximal lipid tail in a hexaacylated agonist (16). To explore these observations further, we carried out molecular simulations for both active (iMD-2c) and inactive (iMD-2o) conformations of the gating loop and for the complete active $[TLR4{\cdot}MD\text{-}2]_2$ complex and measured ligand tail solvent exposure (Fig. 4*A*). For LPA and MPLA, the positions occupied by the lipid tails were relatively stable throughout the simulation (Fig. 3*B*), with the R2 chain remaining solvent-exposed. The oppositely orientated lipid A state, with the glucosamine disaccharide headgroup rotated by 180° (LPAo), was also simulated; in this case, following relaxation of the initial tail conformations (Fig. 3*B*), the R3″ chain remained relatively exposed. Thus, for the hexaacylated ligands, the lipid tail nearest to the cavity mouth was consistently solvent-exposed, typically by approximately ~2–3 times that of the remaining fatty acyl chains. Importantly, this was the case for both the iMD-2c and iMD-2o states, in support of the NMR relaxation data for both wild type and F126A (16). In contrast with the relatively stable tails, the glucosamine disaccharide headgroups were able to shift across the cavity by up to ~0.5 nm, to satisfy direct or counterion-mediated salt bridges with the phosphate groups. In the absence of stabilizing electrostatic interactions with TLR4, the phosphate most distant from the cavity entrance became complexed with residues including Arg-96, Asp-99, Asp-100, and Asp-101 on a highly charged patch of MD-2, whereas the other phosphate tended to interact with Glu-92/Arg-90, resulting in an orientation more similar to the crystal structure of LPIVa-bound iMD-2.

Intriguingly, a similar pattern of lipid tail exposure was observed for the antagonistic and inactive ligands (LPIVa, Erit, and Myr) in iMD-2 as for the agonist-bound state (Fig. 4*A*). It is noteworthy that in all systems, ligand exposure was consis-

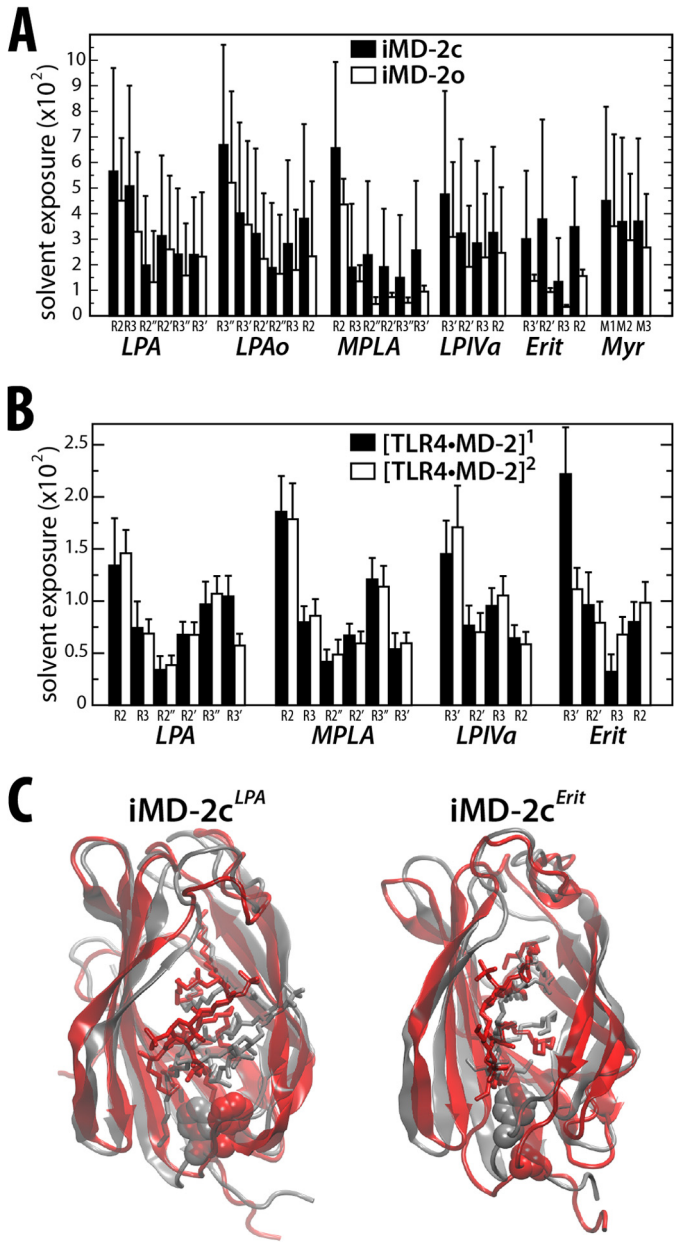

FIGURE 4. **Lipid tail exposure.** Solvent exposure is defined as the mean number of waters within 0.6 nm of each lipid tail. *A* and *B*, histograms are shown for each iMD-2 system (*A*) and for the two symmetry-related MD-2 sites in each $[TLR4{\cdot}MD\text{-}2]_2$ complex system (*B*). The lipid tails on the histogram are listed in order of their proximity to the cavity mouth, from closest (*left*) to furthest (*right*). *C*, the relations between lipid tail exposure and the conformation of Phe-126 (*spacefill* format) of MD-2 (*schematic* format) are *highlighted* for iMD-2^{LPA} (*left*) and iMD-2^{Erit} (*right*), at 0 ns (*gray*) and 100 ns (*red*).

tently greater in the closed gating loop conformation, suggesting that Phe-126 provides a platform to support fatty acyl protrusion. Moreover, although absolute exposure was reduced upon interaction with TLR4, the same overall pattern was again reproduced within the $[TLR4{\cdot}MD\text{-}2]_2$ complex, irrespective of the nature of the bound agonist or antagonist (Fig. 4*B*). In summary, increased solvent exposure, relative to the remainder of the ligand, of the first lipid tail (or single fatty acid chain in the case of Myr) is not dependent upon the conformation of the gating loop or the nature of bound ligand, and precedes receptor association. It is therefore unlikely to be sufficient for TLR4 (in)activation, and hence, other molecular signals must be involved.

The MD-2 Cavity Allosterically Signals to the Gating Loop—Yu *et al.* showed via chemical shift perturbation that the local environment of labeled acyl tails in bound MD-2 agonist is somehow altered by Phe-126 (16). To characterize the behavior of the Phe-126 loop, we aligned the β-strands of simulated MD-2 onto the x-ray structure and then calculated the pairwise root mean square deviation (r.m.s.d.) of the loop Cα atoms; this provides an indication of the relative motion of the loop with respect to the rest of the protein. For iMD-$2c^{LPA}$, this r.m.s.d. was ~0.3 nm (Fig. 5*A*), and the side chain of Phe-126 retained its location for stable interaction with the proximal acyl tails (Fig. 5*C*). This was similar to iMD-$2c^{LPAo}$, consistent with minor NMR cross-peaks observed for the reverse orientation of endotoxin (16). However, all other ligand-bound states exhibited significant destabilization of the closed gating loop conformation, relative to the β-cup fold, with an r.m.s.d. of 0.45–0.5 nm (Fig. 5*A*), including MPLA, whose lack of a 1′-PO_4 "anchor" loosened glucosamine attachment and hence tail stability (Fig. 3) at the cavity mouth. Consequently, partial agonist, antagonist, and inactive ligands induced loss of the Phe-126 conformation common to the agonist-bound state (Fig. 5*C*) prior to receptor association, leading to a loss of interaction with the respective protruding lipid tail (Fig. 4*C*). This was concomitant with a loss of buried surface area (BSA) between the Phe-126 side chain and lipid tails by the end of each simulation, ranging from 1.47 ± 0.15 nm^2 and 1.05 ± 0.30 nm^2 for iMD-$2c^{LPA}$ and iMD-$2c^{LPAo}$, respectively, to just 0.58 ± 0.22 nm^2 for iMD-$2c^{LPIVa}$. Moreover, there was effectively zero BSA observed for iMD-$2c^{MPLA}$ (0.01 ± 0.03 nm^2), iMD-$2c^{Erit}$ (0.01 ± 0.04 nm^2), and iMD-$2c^{Myr}$ (0 ± 0.01 nm^2). Thus, the conformational stability of the active gating loop conformation is reduced in the absence of agonist (see Table 1), supporting the proposal of Yu *et al.* that local rearrangements of this loop may determine the likelihood of receptor complex formation (16).

Although no large scale unfolding was evident (Fig. 5*A*), the strands surrounding the exit to the cavity exhibited local conformational heterogeneity in the absence of agonist, adapting their conformation according to the ligand present (Fig. 6*A*). Careful inspection of the MD-2 cavity over the course of each trajectory revealed that flexing and unfolding of βC-βD and βG-βH (*i.e.* leading into the gating loop), combined with adjustments in the separation between opposing β-sheets, led to significant changes in the internal cavity shape for some systems (Fig. 6*A*). Strikingly, a near perfect correlation was observed between the number of aliphatic carbons present in the fatty acyl tail portion of each ligand and the resultant cavity volume (Fig. 6*B*), for both the closed and open states of MD-2. The internal volume remained close to that of the LPS-bound x-ray structure in the presence of hexaacylated species (~2 nm^3 for LPA, LPAo, and MPLA), shrunk to ~1.5 nm^3 (Erit) and ~1.25 nm^3 (LPIVa) for the tetraacylated ligands, and collapsed to half its original size (~1 nm^3) when housing three myristate fatty acids (see Table 1). Thus, while avoiding major conformational rearrangements, MD-2 is able to sensitively adapt to each respective ligand via clamshell-like motions, adjusting the separation between opposing β-sheets; this is coupled to (de)sta-

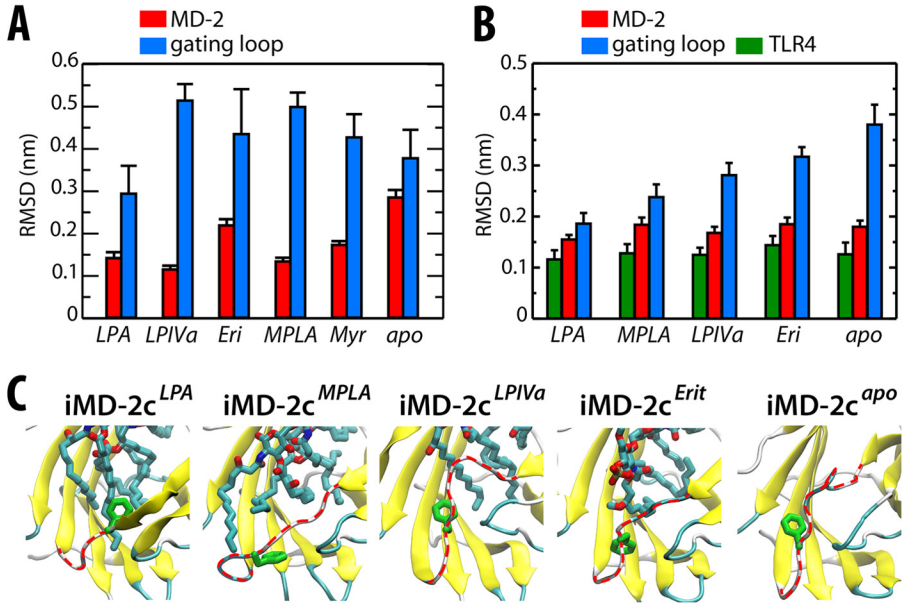

FIGURE 5. **Conformational changes in MD-2.** *A*, mean Cα r.m.s.d. over final 20 ns for all β-strand residues, or for the gating loop, in iMD-2c simulations, relative to the x-ray structure of MD-2 in the active receptor complex. *B*, mean Cα r.m.s.d. for all β-strand residues or gating loop of each MD-2 protein, and for structural regions of each TLR4 chain, over final 20 ns of $[TLR4{\cdot}MD\text{-}2]_2$ simulations, relative to the x-ray structure of MD-2 in the active receptor complex. *C*, final conformation of Phe-126 in iMD-2c simulations; frame chosen according to proximity to the average buried area between Phe-126 and lipid over the final 20 ns. MD-2 is shown in *schematic* representation, with Phe-126 (*green*) and ligand (*CPK colors*) shown in *wireframe* format. The gating loop is *highlighted* in *red-dashed* format.

bilization of β-hairpins at the cavity mouth and consequently, the gating loop, thereby providing a possible mechanism for its role as a "molecular switch" in receptor (de)activation.

MD-2 Plasticity Is Reversible and Reproducible—In the absence of high resolution experimental data it is important to establish the reproducibility and extent of the apparent malleability of the MD-2 β-cup. Thus, 600 ns of additional simulation sampling was generated, split into six independent trajectories, consisting of MD-2 in the closed ($iMD\text{-}2c^{apo}$) or open state ($iMD\text{-}2o^{apo}$), in the absence of any lipid. Three further 100-ns $iMD\text{-}2c^{apo}$ simulations were generated to test force field dependence, using the all-atom AMBER99SB-ILDN (21) and OPLS-AA/L (22) parameters, and the united-atom GROMOS53A6 (23) parameter set. Finally, additional 100-ns control simulations using CHARMM protein parameters with the TIP4P and TIP5P water models were also performed, for which comparable results were obtained (data not shown). In all cases, complete loss of the internal cavity was observed, with the volume initially reducing from ~1.5 nm^3 to ~0.5 nm^3 in the first ~50 ns (Fig. 7*A*), and to ≤0.25 nm^3 toward the end of each simulation, *i.e.* the cavity was effectively absent (Fig. 6*A*). The final conformations of each apo system across force fields closely resembled one another (Fig. 7*B*), exhibiting significant narrowing of the cavity entrance and destabilization of the β-hairpins at the mouth.

Closure in the absence of ligand resulted from hydrophobic collapse of the internal cavity (Fig. 7*C*), with concomitant loss of ~30–40 resident water molecules over the same time scale as cavity closure (Fig. 7*A*). To test the reversibility of this process, the final snapshot from an $iMD\text{-}2c^{apo}$ system was extracted, and six myristate fatty acids were placed a minimum of 1 nm above the cavity opening (Fig. 7*E*). A subsequent simulation of this system ($iMD\text{-}2c^{+Myr}$) led to adsorption of four myristate chains onto the surface of the cavity opening within ~20 ns, a gradual reopening of the protein between 30 and 60 ns as three fatty acyl tails spontaneously tunneled into the hydrophobic core of the cavity, and a final relaxation phase with a mean volume of ~1.1 nm^3 (Fig. 7*D*). It is helpful to compare this with the 100-ns $iMD\text{-}2c^{Myr}$ simulation, based on a crystal structure in which unidentified ligand density was modeled as three myristic acid molecules (14), where a final cavity volume of ~1.2 nm^3 was observed (Fig. 7*D*). Moreover, the backbone r.m.s.d. of the β-cup fold compared with the x-ray structure decreased from ~0.3 nm observed for $iMD\text{-}2c^{apo}$ to ~0.15 nm in the $iMD\text{-}2c^{+Myr}$ simulation over 100 ns, comparable with that observed for $iMD\text{-}2c^{Myr}$. Thus, the extreme malleability of the MD-2 β-cup fold is absolutely reproducible across a range of protein force fields and water models, and it may collapse or expand, depending upon the local presence of hydrophobic molecules.

The MD-2 Allosteric Switch Determines Receptor Complex Stability—To explore the role of the proposed MD-2 allosteric switch within the active receptor complex (13), the stability of LPA-bound $[TLR4{\cdot}MD\text{-}2]_2$ was compared with that in the presence of MPLA, LP4A, Erit, or the lipid-free apo state, in the context of key interaction interfaces at the primary (TLR4·MD-2) and secondary (TLR4*·MD-2) sites (Fig. 1*A*). In all ligand-bound systems, the primary interface was well maintained (Fig. 8*C*), with a constant BSA ≥8 nm^2. This was supported in part by the presence of a salt bridge consistently formed between phosphate and Arg-264 (and in LPA only, Asp-294, via a bridging Na^+ ion that spontaneously bound to this site in the absence of crystallographic Mg^{2+}) (Fig. 8*A*). Even in the ligand-free, apo state, this contact interface was relatively stable, with a BSA ≥7 nm^2, as a result of a series of stable interactions formed between conserved ionizable residues on TLR4

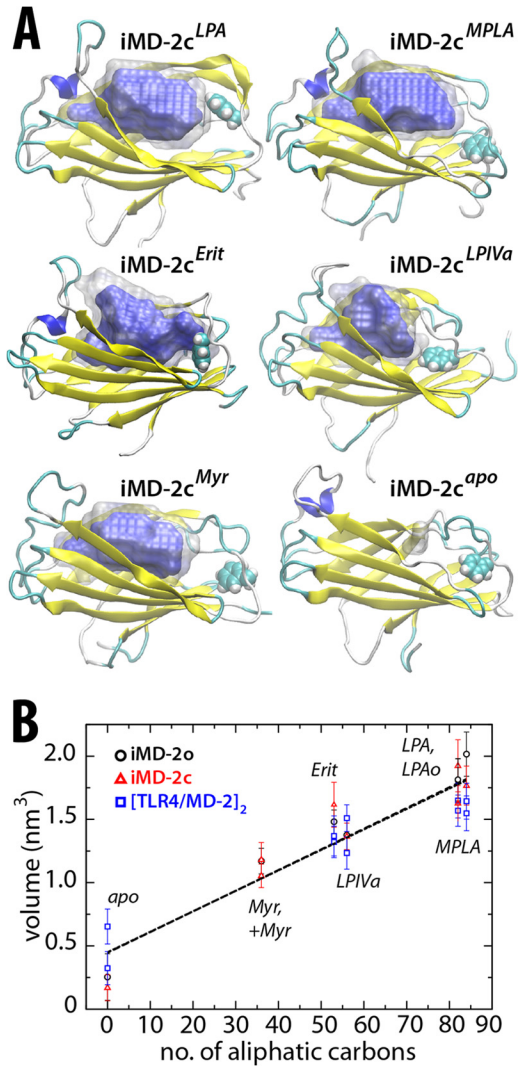

FIGURE 6. **Malleability of the MD-2 cavity.** *A*, mean surface of the internal hydrophobic cavities over the final 20 ns for iMD-2c systems. Cavity surfaces with >90% probability are shown in *blue*, with the equivalent >50% probability overlaid in *transparent gray*. Protein is shown in *schematic* representation, with Phe-126 in *spacefill* format. *B*, correlation between MD-2 cavity volume size and total number of aliphatic carbons within the tail of each bound ligand. $R^2 = 0.95$ for all data points; $R^2 \geq 0.95$ for iMD-2c, iMDo, or [TLR4·MD-2]$_2$ systems only.

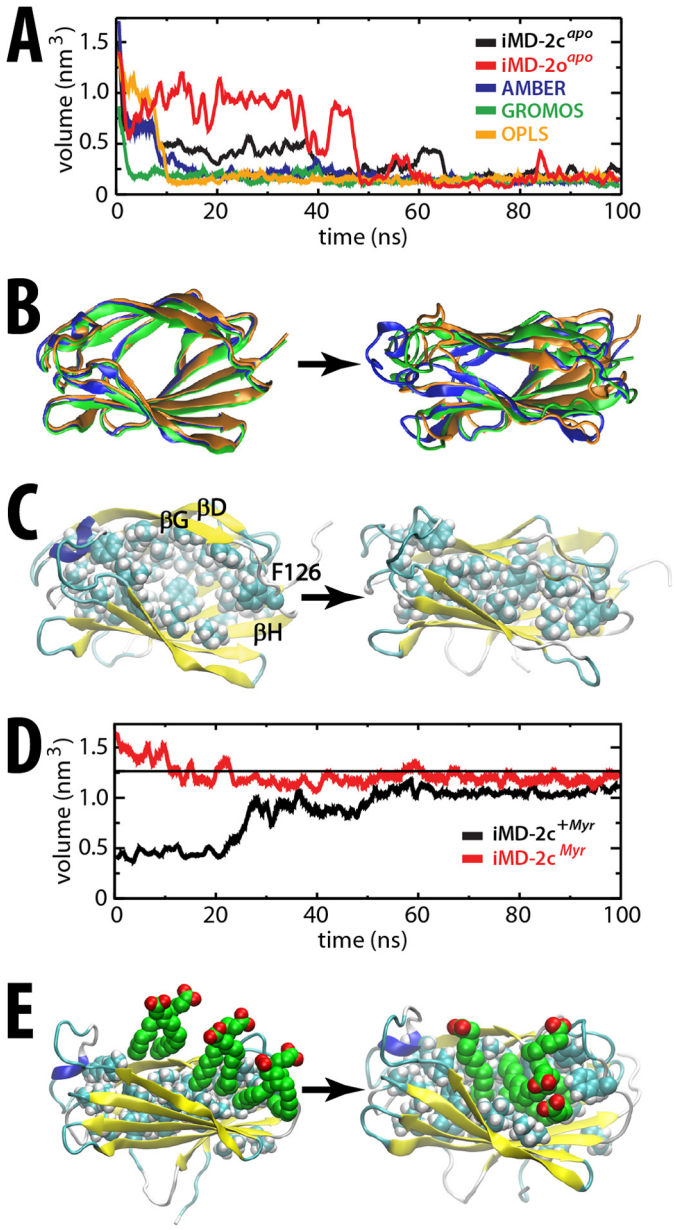

FIGURE 7. **Reproducibility and reversibility of MD-2 conformational plasticity.** *A*, collapse of the binding cavity of ligand-free iMD-2c and iMD-2o with the CHARMM force field over 100 ns compared with that with AMBER, GROMOS, and OPLS. *B*, final MD-2 conformation (shown in *schematic* format) *colored* according to *A*. *C*, starting and final structures of iMD-2c^{apo}, with nonpolar hydrophobic side chains within the cavity shown in *spacefill* format, highlighting the process of hydrophobic collapse. *D* and *E*, change in volume over 100 ns for the experimental myristate-bound iMD-2^{Myr}, compared with collapsed iMD-2c^{apo} upon addition and subsequent binding of myristate (iMD-2^{+Myr}), with initial and final structures highlighted in *E*.

and MD-2 (Fig. 9). Thus, formation of the TLR4·MD-2 heterodimer is not conditional upon the presence of stimulatory endotoxin, consistent with experiment (12).

However, the secondary interface was only consistently stable in the LPA complex, which reproduced key MD-2·TLR4* interactions from the crystallographic LPS-bound structure (13) (Fig. 8*A*) and maintained a BSA of ≥5 nm^2 at both sites (Fig. 8*C*). Destabilization of this interface in the agonist-free systems was somewhat asymmetric with respect to the two TLR4*·MD-2 contact surfaces, with one receptor site apparently compensating for weakening at the other, supported in the context of the relative internal rigidity of the solenoidal TLR4 framework, as observed both in the complex (Fig. 5*B*) and in the isolated TLR4 (iTLR4) state, for which an r.m.s.d. of ≤0.2 nm was observed over ten simulation replicas (data not shown). For example, one of the sites in the MPLA and Erit systems exhibited a reduction in BSA of ~1 and ~3 nm^2, respectively (Fig. 8*C*). Moreover, the LPIVa and apo systems each exhibited a reduction of ~2 nm^2 at one site, and as much as ~4 nm^2 at the other (Fig. 8*C*). This partly resulted from a loss of "tethering" of the glucosamine associated with the more exposed acyl tails, either due to the absence of a 1-PO$_4$ group in MPLA or contraction of the MD-2 cavity in response to tetraacylated Erit and LPIVa (Fig. 6). Thus, in contrast with LPA where its 1-PO$_4$ phosphate group interacted electrostatically with Lys-388 on TLR4*, only the more "buried" phosphate group was consistently coordinated in the agonist-free systems, by Lys-362

TABLE 1
Final ligand-dependent states following simulation of active conformation of isolated MD-2 (iMD-2c) or active receptor complex ([TLR4·MD-2]$_2$)

Ligand description		iMD-2c simulations		[TLR4·MD-2]$_2$ simulations	
Ligand name	Reported activity and structural features	Active gating loop stability[a]	Cavity size[b]	Phe-126 state[c]	Cavity size[b]
			%		%
E. coli lipid A (LPA)	Agonist (6 tails + 2 phosphates)	Stable (intermediate for LPAo)	100	Active (closed)	100
Monphosphoryl lipid A (MPLA)	Partial agonist (6 tails + 1 phosphate)	Unstable	100	Intermediate	100
E. coli lipid IVa (LPIVa)	Weak antagonist (4 tails + 2 phosphates)	Unstable	63	Inactive (open)	63
Eritoran (Erit)	Synthetic antagonist (4 tails + 2 phosphates)	Unstable	75	Inactive (open)	75
Myristate (Myr)	NA[d] (1 tail + carboxylate)	Unstable	50	Inactive (open)	50
No ligand (apo)	NA[d]	Unstable	0	Inactive (open)	NA[e]

[a] Based on measurement of loop r.m.s.d. and Phe-126/lipid buried surface area.
[b] Calculated as a percentage of LPA-bound MD-2.
[c] Based on visual analysis and TLR4*·MD-2 buried surface area.
[d] NA, no experimentally reported activity.

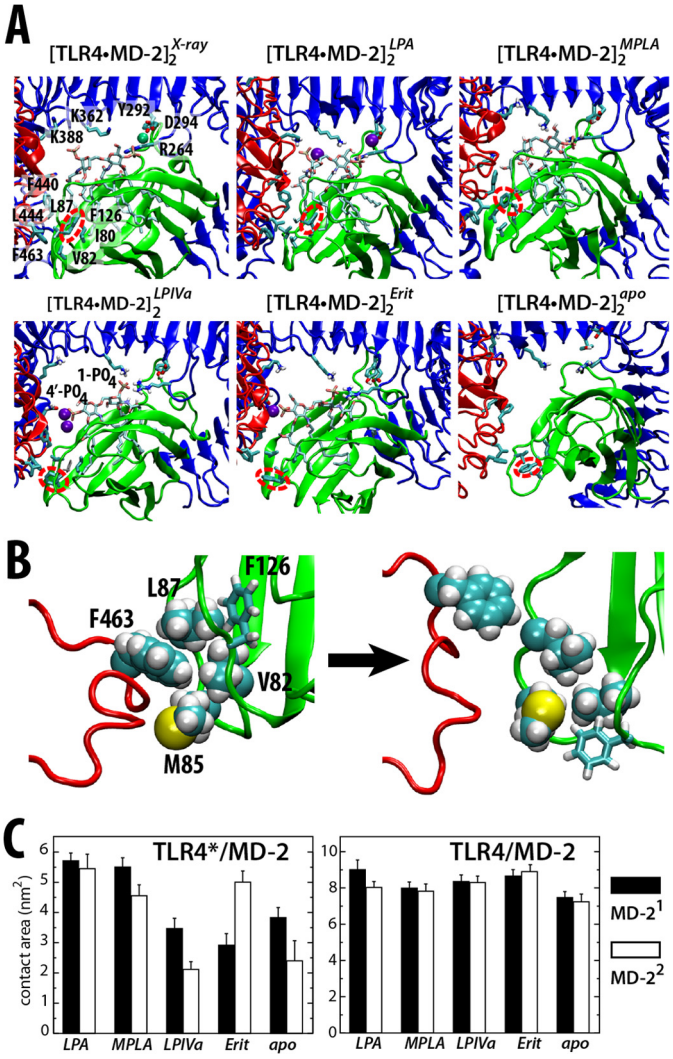

FIGURE 8. **Molecular signaling within the receptor complex.** *A*, the x-ray structure of LPS-bound [TLR4·MD-2]$_2$ at one of the MD-2 bound sites is compared with the final simulation structure of the complex when bound to a range of ligands, or in the ligand-free state. Protein chains are shown in *schematic* representation and *colored* as in Fig. 1, with bound ligand and adsorbed sodium ions in *wireframe* or *spacefill* format, respectively. Key interacting residues are labeled for the x-ray structure. The orientation of Phe-126 is *highlighted* with a *red, dashed ellipse*. *B*, loss of docked, active conformation of Phe-126 (*wireframe* format) and concomitant disruption of TLR4*·MD-2 hydrophobic cluster (*spacefill* format) is highlighted for starting (*left*) and final (*right*) structures of [TLR4·MD-2]$_2^{apo}$. Protein chains are shown in *schematic* representation, *colored* according to *A*. *C*, the mean contact surface area buried between MD-2 and the receptor at the primary and secondary interfaces was calculated over the final 20 ns, each shown for two equivalent sites within the receptor complex.

and/or Lys-341 of the TLR4 chain (Figs. 8*A* and 9); intriguingly, these residues are part of a hypervariable region important for species-dependent specificity (31).

Consistent with the stable cavity volume (Fig. 6*B*) and low structural heterogeneity of the gating loop in [TLR4·MD-2]$_2^{LPA}$ (Fig. 5*B*), the conformation of Phe-126 remained close to that of the x-ray structure, forming a hydrophobic cluster of interactions with the exposed LPA lipid tail along with residues including Ile-80, Val-82, and Leu-87 in MD-2, and Phe-440, Leu-444, and Phe-463 in TLR4* (Figs. 8*A* and 9), supported by a salt bridge formed between nearby Lys-125 of MD-2 and Glu-422 of TLR4*. This is in striking contrast to the agonist-free interfaces; following the reduction in MD-2 cavity volume (Fig. 6) and gating loop stability (Fig. 5*B*), spontaneous reorientation of Phe-126 from the closed to open state was observed to occur, in the presence of LPIVa, Erit, and in the ligand-free apo state (Fig. 8*A* and Table 1). This led to loss of interaction with lipid and destruction of the TLR4*·MD-2 hydrophobic cluster evidently critical for maintaining the receptor heterodimerization interface. In particular, the open orientation of Phe-126 disrupted the arrangement of nearby side chains of Leu-87, Val-82, and Met-85 in MD-2, leading to loss of a pocket that supported the phenyl ring of Phe-463 from TLR4* in the closed state (Fig. 8*B*). In the case of the MPLA system, partial agonist induced a reoriented Phe-126 state that was intermediate between the agonist and antagonist systems (Fig. 8*A*).

DISCUSSION

Our findings help to clarify the molecular signaling mechanism in TLR4, the details of which are consistent with and extend recent observations from biochemical and biophysical experiments. In particular, we have built on the work of Yu *et al.* (16), confirming that lipid tail exposure alone is insufficient for determining formation of the active receptor complex, and showing that tuned (de)stabilization of the gating loop in response to bound ligand influences stability of Phe-126, prior to receptor association. Furthermore, for the first time we observe the spontaneous reorientation of Phe-126 from the closed to open conformation in various agonist-free states of the active receptor complex, with concomitant destabilization of the key TLR4*·MD-2 heterodimeric interface, confirming the role of Phe-126 as a molecular switch. We speculate that this loss of stability at the heterodimeric interface in the absence of agonist would lead to changes in the relative arrangement of TM domains, which play a key functional role

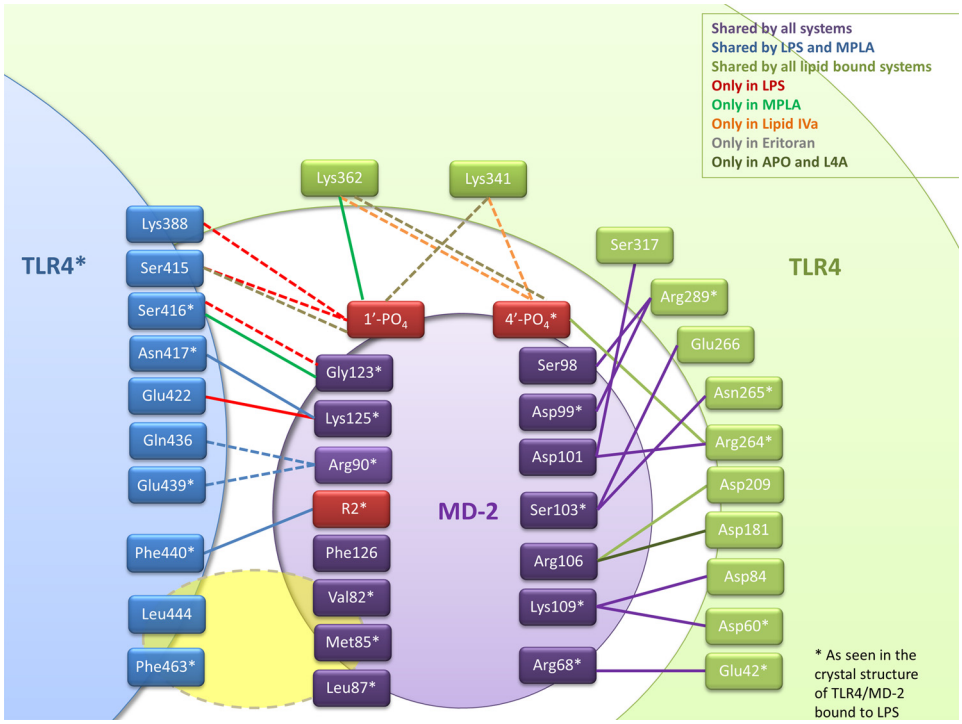

FIGURE 9. **Schematic representation of the common interactions observed within each [TLR4·MD-2]$_2$ system over the final 20 ns of simulation.**

in oligomerization (32–34), and loss of organization of the activated cytoplasmic TIR domain scaffold necessary for recruitment of adaptor proteins and subsequent signaling. Indeed, in comparison with [TLR4·MD-2]$_2^{LPA}$, which maintained the separation found within the x-ray structure (13) between the pair of membrane-proximal carboxyl-terminal regions on each TLR4 chain, all agonist-free systems demonstrated significant divergence from this, by 0.2–0.3 nm. Thus, the conformational plasticity that we observe for each system at the TLR4*·MD-2 interface correlates with the relative arrangement of the carboxyl-terminal regions, in agreement with recent structural data obtained for TLR8 which revealed changes in dimerization interface and carboxyl-terminal separation upon ligand binding (35). However, it should be borne in mind that the time scales associated with downstream signal propagation are likely to be significantly longer than we have sampled in our simulations. To our knowledge, the kinetics of TLR4 assembly and extracellular-to-intracellular signaling is unknown, but almost certainly spans microsecond to millisecond time scales or beyond.

We have also provided evidence that MPLA results in an intermediate level of Phe-126 switching, which may help to explain why it is only able to weakly activate the MAL-MyD88 signaling pathway, due to diminished recruitment of MyD88 to TLR4. Indeed, the resultant, partially destabilized TLR4*·MD-2 interface is consistent with recent data from Casella and Mitchell (36). An antibody assay revealed that MPLA species drove low potency heterotetramerization in comparison with lipid A. However, the signaling capacity of MPLA was reduced by the F126A MD-2 mutant (which allows lipid binding but interferes with active TLR4·MD-2 complex formation), suggesting that an intermediate level of TLR4·MD-2 heterotetramerization is the likely explanation for the weak, biased agonism of MPLA, in agreement with our atomic level observations.

Key to the proposed signaling mechanism is the apparent malleability of the MD-2 scaffold. Its β-cup fold exhibits reversible, clamshell-like motions that enable it to allosterically transmit its ligand-bound state to the Phe-126 molecular switch. Our conclusions have been made on the basis of several protein conformations, a wide variety of ligand-bound states, and multiple simulation replicas of the ligand-free state, using four force fields and three water models. The reproducibility of the conformational plasticity of MD-2 is in partial agreement with previous theoretical studies revealing flexibility around the cavity mouth (37) and collapse of apo MD-2 (38), though no discernible trends with regard to ligands or the gating loop were reported, likely due to the significantly shorter time scales used. Only limited evidence has so far been found for the plasticity of MD-2 from high resolution structural approaches. Comparison of various ligand-bound structures and associated *B*-factors (12–14) at least hints at the potential for flexibility around the mouth of the β-cup, whereas it is possible that the presence of disordered/unidentified hydrophobic ligands within the cavity (14) and extensive crystal lattice contacts may mask the conformational plasticity of MD-2. Significantly, the MD-2-related lipid-recognition family also includes mite allergen proteins such as Der f 2 and Der p 2, for which both collapsed/closed and open experimental structures do exist, separated by clamshell-like motions (39). These conserved dynamics also provide evidence that mite allergenicity may result from TLR4 coercion.

In terms of time scale, the experimental characterization of hydrophobic collapse has typically been hampered by difficulties in isolating the process from other events such as folding. However, Sadqui *et al.* were able to directly follow the dynamics

of hydrophobic collapse in a simple protein, in the absence of competing processes, via fluorescence resonance energy transfer (FRET) measurement between two terminal fluorophores upon a laser-induced temperature jump trigger (40). The relaxation time for hydrophobic collapse at room temperature was on the order of tens of nanoseconds. Moreover, comparable time scales as described here for hydrophobic collapse were recently reported for atomistic simulations of another lipid-binding protein family, CD1, suggesting that this may be a common mechanism in hydrophobic ligand binding and release (41).

From the biomedical viewpoint, our results advocate the importance of considering conformational plasticity when attempting to design novel therapeutic molecules for manipulation of TLR4 signaling pathways. Thus, molecular simulation represents a genuinely useful strategy for predicting the stimulatory outcome of novel compounds, particularly because endotoxic ligands typically possess "non-drug-like" properties. We have demonstrated a striking correlation between the size of the hydrophobic portion of the ligand and cavity volume of MD-2, which should be useful for rapidly estimating the degree of endotoxicity; and we have shown that this directly, but asymmetrically, can determine receptor complex stability and hence activation. Although the time scales sampled here are insufficient to delineate the complete regulatory pathway, if the observed asymmetry of receptor de(activation) is indeed a general feature of TLR4 signaling, this has potential consequences for ligand design, as well as for refinement strategies of crystallographic receptor structures. It is therefore hoped that the knowledge gained from this study will contribute both to understanding receptor signaling mechanisms and to the development of new molecules for pharmacological manipulation of TLRs, as their association with many infectious, allergic, inflammatory and malignant disease continues to intensify (2).

Acknowledgments—We acknowledge the Darwin Supercomputer of the University of Cambridge and the Swiss National Supercomputing Center via DECI/PRACE-2IP. We thank Monique Gangloff and Syma Khalid for helpful discussions.

REFERENCES

1. Akira, S., Uematsu, S., and Takeuchi, O. (2006) Pathogen recognition and innate immunity. *Cell* **124,** 783–801
2. O'Neill, L. A., Bryant, C. E., and Doyle, S. L. (2009) Therapeutic targeting of Toll-like receptors for infectious and inflammatory diseases and cancer. *Pharmacol. Rev.* **61,** 177–197
3. Bryant, C. E., Spring, D. R., Gangloff, M., and Gay, N. J. (2010) The molecular basis of the host response to lipopolysaccharide. *Nat. Rev. Microbiol.* **8,** 8–14
4. Gioannini, T. L., Teghanemt, A., Zhang, D., Coussens, N. P., Dockstader, W., Ramaswamy, S., and Weiss, J. P. (2004) Isolation of an endotoxin-MD-2 complex that produces Toll-like receptor 4-dependent cell activation at picomolar concentrations. *Proc. Natl. Acad. Sci. U.S.A.* **101,** 4186–4191
5. Núñez Miguel, R., Wong, J., Westoll, J. F., Brooks, H. J., O'Neill, L. A., Gay, N. J., Bryant, C. E., and Monie, T. P. (2007) A dimer of the Toll-like receptor 4 cytoplasmic domain provides a specific scaffold for the recruitment of signalling adaptor proteins. *PLoS One* **2,** e788
6. Zähringer, U., Lindner, B., and Rietschel, E. T. (1994) Molecular structure of lipid A, the endotoxic center of bacterial lipopolysaccharides. *Adv. Carbohydr. Chem. Biochem.* **50,** 211–276
7. Walsh, C., Gangloff, M., Monie, T., Smyth, T., Wei, B., McKinley, T. J., Maskell, D., Gay, N., and Bryant, C. (2008) Elucidation of the MD-2/TLR4 interface required for signaling by lipid IVa. *J. Immunol.* **181,** 1245–1254
8. Golenbock, D. T., Hampton, R. Y., Qureshi, N., Takayama, K., and Raetz, C. R. (1991) Lipid A-like molecules that antagonize the effects of endotoxins on human monocytes. *J. Biol. Chem.* **266,** 19490–19498
9. Figueiredo, M. D., Moore, J. N., Vandenplas, M. L., Sun, W. C., and Murray, T. F. (2008) Effects of the second-generation synthetic lipid A analogue E5564 on responses to endotoxin in [corrected] equine whole blood and monocytes. *Am. J. Vet. Res.* **69,** 796–803
10. Mullarkey, M., Rose, J. R., Bristol, J., Kawata, T., Kimura, A., Kobayashi, S., Przetak, M., Chow, J., Gusovsky, F., Christ, W. J., and Rossignol, D. P. (2003) Inhibition of endotoxin response by e5564, a novel Toll-like receptor 4-directed endotoxin antagonist. *J. Pharmacol. Exp. Ther.* **304,** 1093–1102
11. Mata-Haro, V., Cekic, C., Martin, M., Chilton, P. M., Casella, C. R., and Mitchell, T. C. (2007) The vaccine adjuvant monophosphoryl lipid A as a TRIF-biased agonist of TLR4. *Science* **316,** 1628–1632
12. Kim, H. M., Park, B. S., Kim, J. I., Kim, S. E., Lee, J., Oh, S. C., Enkhbayar, P., Matsushima, N., Lee, H., Yoo, O. J., and Lee, J. O. (2007) Crystal structure of the TLR4-MD-2 complex with bound endotoxin antagonist Eritoran. *Cell* **130,** 906–917
13. Park, B. S., Song, D. H., Kim, H. M., Choi, B. S., Lee, H., and Lee, J. O. (2009) The structural basis of lipopolysaccharide recognition by the TLR4-MD-2 complex. *Nature* **458,** 1191–1195
14. Ohto, U., Fukase, K., Miyake, K., and Satow, Y. (2007) Crystal structures of human MD-2 and its complex with antiendotoxic lipid IVa. *Science* **316,** 1632–1634
15. Teghanemt, A., Re, F., Prohinar, P., Widstrom, R., Gioannini, T. L., and Weiss, J. P. (2008) Novel roles in human MD-2 of phenylalanines 121 and 126 and tyrosine 131 in activation of Toll-like receptor 4 by endotoxin. *J. Biol. Chem.* **283,** 1257–1266
16. Yu, L., Phillips, R. L., Zhang, D., Teghanemt, A., Weiss, J. P., and Gioannini, T. L. (2012) NMR studies of hexaacylated endotoxin bound to wild-type and F126A mutant MD-2 and MD-2.TLR4 ectodomain complexes. *J. Biol. Chem.* **287,** 16346–16355
17. Hess, B., Kutzner, C., Van der Spoel, D., and Lindahl, E. (2008) GROMACS 4: Algorithms for highly efficient, load-balanced, and scalable molecular simulation. *J. Chem. Theory Comput.* **4,** 435–447
18. MacKerell, A. D., Bashford, D., Bellott, Dunbrack, R. L., Evanseck, J. D., Field, M. J., Fischer, S., Gao, J., Guo, H., Ha, S., Joseph-McCarthy, D., Kuchnir, L., Kuczera, K., Lau, F. T. K., Mattos, C., Michnick, S., Ngo, T., Nguyen, D. T., Prodhom, B., Reiher, W. E., Roux, B., Schlenkrich, M., Smith, J. C., Stote, R., Straub, J., Watanabe, M., Wiorkiewicz-Kuczera, J., Yin, D., and Karplus, M. (1998) All-atom empirical potential for molecular modeling and dynamics studies of proteins. *J. Phys. Chem. B.* **102,** 3586–3616
19. Bjelkmar, P., Larsson, P., Cuendet, M. A., Hess, B., and Lindahl, E. (2010) Implementation of the CHARMM force field in GROMACS: analysis of protein stability effects from correction maps, virtual interaction sites, and water models. *J. Chem. Theory Comput.* **6,** 459–466
20. Piggot, T. J., Holdbrook, D. A., and Khalid, S. (2011) Electroporation of the *E. coli* and *S. aureus* membranes: molecular dynamics simulations of complex bacterial membranes. *J. Phys. Chem. B.* **115,** 13381–13388
21. Lindorff-Larsen, K., Piana, S., Palmo, K., Maragakis, P., Klepeis, J. L., Dror, R. O., and Shaw, D. E. (2010) Improved side-chain torsion potentials for the Amber ff99SB protein force field. *Proteins* **78,** 1950–1958
22. Kaminski, G. A., Friesner, R. A., Tirado-Rives, J., and Jorgensen, W. L. (2001) Evaluation and reparametrization of the OPLS-AA force field for proteins via comparison with accurate quantum chemical calculations on peptides. *J. Phys. Chem. B* **105,** 6474–6487
23. Oostenbrink, C., Villa, A., Mark, A. E., and van Gunsteren, W. F. (2004) A biomolecular force field based on the free enthalpy of hydration and solvation: the GROMOS force-field parameter sets 53A5 and 53A6. *J. Comput. Chem.* **25,** 1656–1676
24. Bussi, G., Donadio, D., and Parrinello, M. (2007) Canonical sampling through velocity rescaling. *J. Chem. Phys.* 126:014101

25. Parrinello, M., and Rahman, A. (1981) Polymorphic transitions in single crystals: a new molecular dynamics method. *J. Appl. Phys.* **52,** 7182–7190
26. Nosé, S., and Klein, M. L. (1983) Constant pressure molecular dynamics for molecular systems. *Mol. Phys.* **50,** 1055–1076
27. Hess, B., Bekker, H., Berendsen, H. J., and Fraaije, J. G. (1997) LINCS: a linear constraint solver for molecular simulations. *J. Comput. Chem.* **18,** 1463–1472
28. Essmann, U., Perera, L., Berkowitz, M. L., Darden, T., Lee, H., and Pedersen, L. G. (1995) A smooth particle mesh Ewald method. *J. Chem. Phys.* **103,** 8577–8593
29. Humphrey, W., Dalke, A., and Schulten, K. (1996) VMD: visual molecular dynamics. *J. Mol. Graph.* **14,** 33–38, 27–38
30. Russell, R. B., and Barton, G. J. (1992) Multiple protein sequence alignment from tertiary structure comparison: assignment of global and residue confidence levels. *Proteins* **14,** 309–323
31. Hajjar, A. M., Ernst, R. K., Tsai, J. H., Wilson, C. B., and Miller, S. I. (2002) Human Toll-like receptor 4 recognizes host-specific LPS modifications. *Nat. Immunol.* **3,** 354–359
32. Nguyen, T. H., Mai, N. L., Le, T. P., Ha, V., Nguyen, T. C., Tran, T. H., Nguyen, T. H., Farrar, J. J., and Dunstan, S. J. (2009) Toll-like receptor 4 (TLR4) and typhoid fever in Vietnam. *PLoS One* **4,** e4800
33. Nishiya, T., Kajita, E., and Miwa, S. (2006) Ligand-independent oligomerization of TLR4 regulated by a short hydrophobic region adjacent to the transmembrane domain. *Biochim. Biophys. Res. Commun.* **341,** 1128–1134
34. Godfroy, J. I., 3rd, Roostan, M., Moroz, Y. S., Korendovych, I. V., and Yin, H. (2012) Isolated Toll-like receptor transmembrane domains are capable of oligomerization. *PLoS One* **7,** e48875
35. Tanji, H., Ohto, U., Shibata, T., Miyake, K., and Shimizu, T. (2013) Structural reorganization of the Toll-like receptor 8 dimer induced by agonistic ligands. *Science* **339,** 1426–1429
36. Casella, C. R., and Mitchell, T. C. (2013) Inefficient TLR4/MD-2 heterotetramerization by monophosphoryl lipid A. *PLoS One* **8,** e62622
37. DeMarco, M. L., and Woods, R. J. (2011) From agonist to antagonist: structure and dynamics of innate immune glycoprotein MD-2 upon recognition of variably acylated bacterial endotoxins. *Mol. Immunol.* **49,** 124–133
38. Garate, J. A., and Oostenbrink, C. (2013) Lipid A from lipopolysaccharide recognition: structure, dynamics and cooperativity by molecular dynamics simulations. *Proteins* **81,** 658–674
39. Ichikawa, S., Takai, T., Inoue, T., Yuuki, T., Okumura, Y., Ogura, K., Inagaki, F., and Hatanaka, H. (2005) NMR study on the major mite allergen Der f 2: its refined tertiary structure, epitopes for monoclonal antibodies and characteristics shared by ML protein group members. *J. Biochem.* **137,** 255–263
40. Sadqi, M., Lapidus, L. J., and Muñoz, V. (2003) How fast is protein hydrophobic collapse? *Proc. Natl. Acad. Sci. U.S.A.* **100,** 12117–12122
41. Garzón, D., Anselmi, C., Bond, P. J., and Faraldo-Gómez, J. D. (2013) Dynamics of the antigen-binding grooves in CD1 proteins: reversible hydrophobic collapse in the lipid-free state. *J. Biol. Chem.* **288,** 19528–19536